

Unified Distributed Control of Stand-Alone DC Microgrids

Zhaojian Wang^D, *Student Member, IEEE*, Feng Liu^{ID}, *Member, IEEE*, Ying Chen, *Member, IEEE*, Steven H. Low, *Fellow, IEEE*, and Shengwei Mei, *Fellow, IEEE*

Abstract—Stand-alone direct current (dc) microgrids may belong to different owners and adopt various control strategies. This brings great challenge to its optimal operation due to the difficulty of implementing a unified control. This paper addresses the distributed optimal control of dc microgrids, which intends to break the restriction of diversity to some extent. First, we formulate the optimal power flow problem of stand-alone dc microgrids as an exact second-order cone program and prove the uniqueness of the optimal solution. Then a dynamic solving algorithm based on primal-dual decomposition method is proposed, the convergence of which is proved theoretically as well as the optimality of its equilibrium point. It should be stressed that the algorithm can provide control commands for the three types of microgrids: 1) power control; 2) voltage control; and 3) droop control. This implies that each microgrid does not need to change its original control strategy in practice, which is less influenced by the diversity of microgrids. Moreover, the control commands for power controlled and voltage controlled microgrids satisfy generation limits and voltage limits in both transient process and steady state. Finally, a six-microgrid dc system based on the microgrid benchmark is adopted to validate the effectiveness and plug-n-play property of our designs.

Index Terms—Distributed control, DC microgrid, optimal power flow, diversity restriction, transient constraint.

I. INTRODUCTION

MICROGRIDS are clusters of distributed generators (DGs), energy storage systems (ESSs) and loads, which are generally categorized into two types: alternating current (AC) and direct current (DC) microgrids [1], [2]. In the past decade, research has been concentrated on enhancing

Manuscript received July 7, 2017; revised August 14, 2017; accepted September 19, 2017. Date of publication September 28, 2017; date of current version December 19, 2018. This work was supported in part by the National Natural Science Foundation of China under Grant 51677100, Grant 51377092, and Grant 51621065, in part by the U.S. National Science Foundation under Award EPCN 1619352, Award CCF 1637598, and Award CNS 1545096, in part by ARPA-E under Award DE-AR0000699, and in part by the Skoltech through Collaboration Agreement under Grant 1075-MRA. Paper no. TSG-00944-2017. (Corresponding author: Feng Liu.)

Z. Wang, F. Liu, Y. Chen, and S. Mei are with the State Key Laboratory of Power Systems and Department of Electrical Engineering, Tsinghua University, Beijing 100084, China (e-mail: zj-wang13@mails.tsinghua.edu.cn; lfeng@tsinghua.edu.cn; chen_ying@tsinghua.edu.cn; meishengwei@tsinghua.edu.cn).

S. H. Low is with the Department of Electrical Engineering, California Institute of Technology, Pasadena, CA 91105 USA (e-mail: slow@caltech.edu).

Color versions of one or more of the figures in this paper are available online at <http://ieeexplore.ieee.org>.

Digital Object Identifier 10.1109/TSG.2017.2757498

the performance of AC microgrids. However, some generations and loads are inherently DC, such as photo-voltaic (PV), battery, computer and electrical vehicle (EV) [3]–[5]. DC microgrids more naturally integrate them and can eliminate unnecessary conversion processes, which improves system efficiency and reliability. In addition, DC systems do not face problems such as reactive power compensation, frequency stability and synchronization [3], which makes it more and more popular in power system. In DC microgrids, hierarchical control is often utilized [6], [7], i.e., primary control, secondary control and tertiary control, which can be implemented in either a centralized manner or a distributed manner. In the centralized manner, a control center is needed to accumulate information from microgrids, compute command and send it back to them. With the increasing number of microgrids as well as uncertainties of renewable generations and load demands, centralized control faces a great challenge, i.e., it is less and less applicable due to problems, e.g., single point failures, heavy communication burden of control center and lack of ability to respond rapidly enough [8]. These problems highlight the need for a distributed control strategy that will require no control center and less communication. This paper addresses this need.

In the hierarchical control architecture, the primary control is almost decentralized. The most popular control manner is the droop control [6], [9], where load sharing is mainly determined by the droop coefficient. As pointed out in [10] and [11], droop control cannot achieve proper load sharing sometimes, especially in systems with unequal resistances and different modes. Many improvements are investigated [10]–[14]. Taking into consideration the effect of different line impedances, [10] proposes a decentralized control strategy to achieve perfect power sharing. In [11], a mode-adaptive decentralized control strategy is proposed for the power management in DC microgrid, which enlarges the control freedom compared with the conventional droop control. In [14], a decentralized method is proposed to adjust the droop coefficient by the state-of-charge of storage, which can achieve equal load sharing. However, similar to the AC power system, primary control in DC system suffers from voltage deviation in the steady state.

To eliminate the voltage deviation, distributed secondary control is developed. The most widely used method is consensus based control [15], where there is usually a global control variable, e.g., global voltage deviation, while each agent only has its local estimation. In the DC system, each agent may

represent a DG or a microgrid. By exchanging information with neighbors, the value of the variable will be identical for all agents finally [7], [16]–[18]. In [7], each microgrid uses dynamic consensus protocol to estimate the global averaged voltage with the local and neighboring estimation. Then, the estimated voltage is compared with the reference value and fed to a PI controller to eliminate the voltage deviation. This method is further improved in [17] by adding a current consensus regulator, where the control goal is to achieve globally identical current ratio compared with the rated current of each microgrid. By doing so, the equal load sharing can be obtained. The discrete consensus method is used in [18] to restore average voltage with accurate load sharing. The consensus based secondary control can realize equality among agents, however, the results may not be optimal.

Tertiary control is to achieve the optimal operation by controlling the power flow among microgrids or among DGs within a microgrid [19]–[21]. Conventionally, tertiary control provides reference operation point for the system. Its time scale is much slower than real time control. However, values of renewable generations and loads may change rapidly due to uncertainties, which makes reference point obtained by tertiary control sub-optimal in the new situation. This requires us to combine real-time coordination and steady-state optimization together, i.e., the optimization solution should be sent to the system in real time. Similar works are given in both AC system [22]–[24] and DC system [25]–[27]. The critical thought in [25]–[27] is that the incremental generation cost of each microgrid is identical in the steady state. In [25], economic dispatch problem is formulated and the incremental generation cost is regarded as a consensus variable. Using the consensus method, the incremental generation cost will be identical in the steady state, and optimality is achieved. Similar method is also used in [27], where the sub-gradient is added to the consensus approach in order to accelerate the convergence. These works are very inspiring in combination of optimal operation and real time control, but they still have some restrictions. For example, the original control strategy of a microgrid has to be revised to the proposed method, which is hard to apply as microgrids may belong to different owners and adopt various control strategies. These problems highlight the need for a distributed control strategy that is less influenced by the diversity.

In this paper, we investigate the distributed optimal power flow control among stand-alone DC microgrids, which is less influenced by their original control strategies. Theoretically, we construct an optimal power flow (OPF) model for stand-alone microgrids with an exact SOCP relaxation and further prove the uniqueness of its optimal solution. By using the primal-dual decomposition method, a distributed dynamic algorithm is proposed, where we also prove its convergence and optimality of its equilibrium point. In the application point of view, the algorithm provides control commands for different control strategies such as power control, voltage control and droop control. This implies that we do not change the original control schemes of microgrids, which breaks the restriction of microgrid diversity. In addition, constraints of generation capacity limits and voltage limits are enforced even in the

transient process of control commands, which implies power commands are always feasible and voltage commands are safe for converters. In this regards, it increases the security of DC system. The contributions of this paper have following aspects:

- The OPF model of stand-alone DC power system is formulated, and the uniqueness of its optimal solution is proved.
- A fully distributed algorithm is proposed to achieve the optimal solution of the OPF problem, where only communications with neighbors are needed with minimal communication burden.
- The proposed method does not change the original control strategy of each DG, which adapts to three most common control modes: power control, voltage control and droop control, breaking restriction of microgrid diversity.
- The control commands for power controlled and voltage controlled microgrids satisfy generation limits and voltage limits in both transient process and steady state.

The rest of the paper is organized as follows. In Section II, network model of DC microgrids is introduced. In Section III, OPF model for stand-alone DC microgrids is formulated. In Section IV, the dynamic algorithm is proposed, the optimality and convergence of the algorithm are proved theoretically. The implementation approach is designed in Section V. Case studies are given in Section VI. Finally, Section VII concludes the paper.

II. NETWORK MODEL

A stand-alone DC system is composed of a cluster of microgrids connected by lines. Each microgrid is treated as a bus with generation and load. Then the whole system is modeled as a connected graph $\mathcal{G} := (\mathcal{N}, \mathcal{E})$, where $\mathcal{N} = \{1, 2, \dots, n\}$ is the set of microgrids and $\mathcal{E} \subseteq \mathcal{N} \times \mathcal{N}$ is the set of lines. If two microgrids i and k are connected by a tie line directly, we denote $(i, k) \in \mathcal{E}$, and abbreviated by $i \sim k$. The resistance of line (i, k) is r_{ik} . The power flow from microgrid i to microgrid k is P_{ik} , and the current from microgrids i to k is I_{ik} . Let $m := |\mathcal{E}|$ be the number of lines.

For each microgrid $i \in \mathcal{N}$, let $p_i^g(t)$ denote the generation at time t and p_i^d denotes its constant load demand. Denote the voltage at bus i as V_i . DGs in the DC microgrids may have different control strategies, such as power control, voltage control and droop control. Power control and voltage control only require their reference values, which are not introduced here in detail. Droop control takes the form:

$$v_i - v_i^* = -k_i(p_i^g - \hat{p}_i). \quad (1)$$

where $v_i = V_i^2$, $k_i > 0$ is the droop coefficient, v_i^* is the voltage square reference, and k_i, v_i^* are constants. \hat{p}_i is the power when $v_i = v_i^*$, which is a variable in the rest of the paper.

Denote the current in line (i, k) from i to k as I_{ik} , which is defined

$$I_{ik} = (V_i - V_k)/r_{ik} \quad (2)$$

Then the power P_{ik} from i to k is

$$P_{ik} = V_i I_{ik} = V_i (V_i - V_k)/r_{ik} \quad (3)$$

Consequently, the power balance in one node is

$$p_i^g - p_i^d = V_i \sum_{k:k \in N_i} (V_i - V_k) / r_{ik} \quad (4a)$$

$$= \sum_{k:k \in N_i} P_{ik}. \quad (4b)$$

where N_i is the set of microgrids connected with microgrid i directly. Our goal is to provide control commands for microgrids adopting different control strategies, which must satisfy the operational constraints:

$$0 \leq p_i^g \leq \bar{p}_i^g \quad (5a)$$

$$\underline{V}_i \leq V_i \leq \bar{V}_i \quad (5b)$$

where \bar{p}_i^g is the upper limit of generation in DG i , $\underline{V}_i, \bar{V}_i$ are lower and upper limits of voltage. For power controlled DG, (5a) is a hard limit, which must be satisfied even during the transient process. Otherwise it is non-executable. For voltage controlled DG, (5b) is not a hard limit, but it also should be satisfied during the transient. This is because overlimit voltage is not secure for the converter nor the operator.

III. OPTIMAL POWER FLOW PROBLEM

A. OPF Model

Existing OPF models are mainly for grid-connected DC system [28]. However, DC microgrids also operate in isolated mode in many situations such as in remote areas or islands. In terms of this, we formulate the ordinary OPF in the stand-alone DC power system.

$$\text{OPF: } \min_{p^g, v, W} \quad f = \sum_{i \in \mathcal{N}} f_i(p_i^g) \quad (6a)$$

s. t. (5a)

$$\underline{V}_i^2 \leq v_i \leq \bar{V}_i^2, \quad i \in \mathcal{N} \quad (6b)$$

$$p_i^g - p_i^d = \sum_{k:k \sim i} (v_i - W_{ik}) / r_{ik}, \quad i \in \mathcal{N} \quad (6c)$$

$$W_{ik} \geq 0, \quad i \sim k \quad (6d)$$

$$W_{ik} = W_{ki}, \quad i \sim k \quad (6e)$$

$$R_{ik} \succeq 0, \quad i \sim k \quad (6f)$$

$$\text{rank}(R_{ik}) = 1, \quad i \sim k \quad (6g)$$

where $R_{ik} = \begin{bmatrix} v_i & W_{ik} \\ W_{ki} & v_j \end{bmatrix}$. If $\text{rank}(R_{ik}) = 1$ always holds, W_{ik} can be divided into $W_{ik} = V_i V_k$. The cost (6a) is a function of generation in each node, which should satisfy

A1: $f_i(p_i^g)$ is strictly increasing when $p_i^g \geq -p_i^d$ for $i \in \mathcal{N}$, second order continuously differentiable and strongly convex ($f_i''(p_i^g) \geq \alpha > 0$).

Constraint (6b) is derived from (5b), and (6c) is from (4a). Constraint (6f) implies matrix R_{ik} is positive semi-definite, and (6g) guarantees the rank of R_{ik} be 1. The difference between (6) and OPF' in [28] is that there is no substation node with fixed voltage in (6). Equation (6) is not convex due to constraint (6g). Remove (6g), and we get the SOCP relaxation of (6).

$$\text{SOCP: } \min_{p^g, v, W} \quad \sum_{i \in \mathcal{N}} f_i(p_i^g)$$

s. t. (5a), (6b)–(6f)

It has been proved in [29] that the relaxation is exact provided that: 1) $\bar{V}_1 = \bar{V}_2 = \dots = \bar{V}_n$; 2) $p_i^d > 0$; 3) $\sum_{i \in \mathcal{N}} (p_i^g - p_i^d) > 0$; 4) $f_i(p_i^g)$ is strictly increasing when $p_i^g \geq p_i^d$ for $i \in \mathcal{N}$. In this paper, conditions 1), 2), 3) are satisfied. With assumption A1, 4) is also satisfied.

To improve the numerical stability of the SOCP, we have the following stable SOCP problem.

$$\text{SSOCP: } \min_{p^g, P, l, v} \quad \sum_{i \in \mathcal{N}} f_i(p_i^g) \quad (7a)$$

s. t. (4b), (5a)

$$P_{ik} + P_{ki} = r_{ik} l_{ik}, \quad i \sim k \quad (7b)$$

$$v_i - v_k = r_{ik} (P_{ik} - P_{ki}), \quad i \sim k \quad (7c)$$

$$l_{ik} \geq P_{ik}^2 / v_i, \quad i \sim k \quad (7d)$$

$$\underline{V}_i^2 \leq v_i \leq \bar{V}_i^2, \quad i \in \mathcal{N} \quad (7e)$$

where $l_{ik} = |I_{ik}|^2$ are squared line currents, and $l_{ik} = l_{ki}$. Constraint (7d) is the SOCP relaxed form. The detailed explanation of (7b)–(7d) is found in [28], which is omitted here.

According to [28, Th. 5], SOCP and SSOCP are equivalent, i.e., there exists a one-to-one map between the feasible set of SOCP and the feasible set of SSOCP, which is

$$\begin{aligned} P_{ik} &= (v_i - W_{ik}) / r_{ik}, \quad i \sim k \\ l_{ik} &= (v_i - W_{ik} - W_{ki} + v_k) / r_{ik}^2, \quad i \sim k. \end{aligned} \quad (8)$$

In some microgrids, droop control is utilized. However, the solution of (7) cannot guarantee v_i and p_i^g satisfy (1), which implies that the optimal solution may not be achieved in reality. In this regard, we add droop control to the constraints, then the problem becomes

$$\text{DSOCP: } \min_{p^g, P, l, v, \hat{p}} \quad \sum_{i \in \mathcal{N}} f_i(p_i^g)$$

s. t. (1), (4b), (5a), (7b)–(7e)

In DSOCP, \hat{p} is an optimization variable, making DSOCP a convex problem.

To help design the algorithm, an equivalent optimization problem is formulated.

$$\text{ESOCP: } \min_{p^g, P, l, v, \hat{p}} \quad \sum_{i \in \mathcal{N}} f_i(p_i^g) + \sum_{i \in \mathcal{N}} \frac{1}{2} y_i^2 + \sum_{i \in \mathcal{N}} \frac{1}{2} z_i^2$$

s. t. (1), (4b), (5a), (7b)–(7e)

where $y_i = v_i + k_i p_i^g - v_i^* - k_i \hat{p}_i$, $z_i = p_i^g - p_i^d - \sum_{k:k \in N_i} P_{ik}$.

Since for any feasible solution of ESOCP we all have $y_i = z_i = 0$, ESOCP is equivalent to DSOCP. y_i and z_i are only put here to accelerate the convergence of the algorithm [30].

B. Uniqueness of Optimal Solution

Before introducing the results, we give an assumption.

A2: The OPF (6) is feasible.

Then, we have the following theorem.

Theorem 1: Suppose A1 and A2 hold. The optimal solution of SSOCP is unique.

The proof of Theorem 1 is given in Appendix A.

Theorem 2: Denote the optimal solution of SSOCP as $x^{1*} = (p^{g1*}, P^{1*}, l^{1*}, v^{1*})$ and the optimal solution of DSOCP as $x^{2*} = (p^{g2*}, P^{2*}, l^{2*}, v^{2*}, \hat{p}^{2*})$. Then,

- 1) there exists an unique \hat{p}^{2*} making (x^{1*}, \hat{p}^{2*}) the optimal solution of DSOCP;
- 2) the optimal solution of DSOCP is unique;
- 3) $(p^{g2*}, P^{2*}, l^{2*}, v^{2*}) = (p^{g1*}, P^{1*}, l^{1*}, v^{1*})$.

The proof of Theorem 2 is given in Appendix A.

Suppose the optimal solution of DSOCP is $x^{2*} = (p^{g2*}, P^{2*}, l^{2*}, v^{2*}, \hat{p}^{2*})$ with the droop coefficient k_{i1} . From the proof of 1) in Theorem 2, if k_{i1} changes to k_{i2} , there exists an unique $\hat{p}^{2*}(k_{i2})$ making $(p^{g2*}, P^{2*}, l^{2*}, v^{2*}, \hat{p}^{2*}(k_{i2}))$ be the optimal solution of DSOCP. This implies that droop coefficient does not influence the optimal solution of SSOCP.

Lemma 1: Optimization problem ESOCP and DSOCP have identical feasible solutions.

It is easy to prove Lemma 1 as $y_i = 0$ and $z_i = 0$ for any feasible solution.

Remark 1: From Theorem 2, it is shown that the unique optimal solution still exists even if droop control is considered, and we can obtain the optimal \hat{p}_2^* . Moreover, for these microgrids that do not adopt droop control, ESOCP can provide the optimal output power and voltage references. In addition, for different droop coefficient k_i , $(p_2^{g*}, P_2^*, l_2^*, v_2^*)$ in the optimal solution does not change. Thus, for microgrids that do not adopt droop control, we can just assign an imaginary droop control to them when formulating ESOCP, i.e., assuming all the microgrids adopt droop control when building ESOCP. This does not influence the optimal solution of these microgrids adopting power control and voltage control. In this regard, our method adapts to three different control strategies.

IV. CONTROL SCHEME DESIGN

A. Distributed Algorithm

Based on the primal-dual algorithm, we propose the following distributed approach to solve the ESOCP, which is

$$\dot{p}_i^g = [p_i^g - (G_i(p_i^g) - \mu_i + k_i \epsilon_i + z_i + k_i y_i)]_0^{\bar{p}_i^g} - p_i^g \quad (9a)$$

$$\dot{v}_i = \left[v_i - \left(y_i + \sum_{k \in N_i} \gamma_{ik} + \epsilon_i - \sum_{k \in N_i} \rho_{ik} \frac{P_{ik}^2}{v_i^2} \right) \right]_{V_i^2}^{\bar{V}_i^2} - v_i \quad (9b)$$

$$\dot{P}_{ik} = -(\mu_i + \lambda_{ik} - \gamma_{ik} r_{ik} + 2\rho_{ik} P_{ik}/v_i - z_i) \quad (9c)$$

$$\dot{l}_{ik} = -(-\lambda_{ik} r_{ik} - \rho_{ik} - \rho_{ki}) \quad (9d)$$

$$\dot{\hat{p}}_i = k_i \epsilon_i + k_i y_i \quad (9e)$$

$$\dot{\mu}_i = - \left(p_i^g - p_i^d - \sum_{k \in N_i} P_{ik} \right) \quad (9f)$$

$$\dot{\epsilon}_i = v_i + k_i p_i^g - v_i^* - k_i \hat{p}_i \quad (9g)$$

$$\dot{\lambda}_{ik} = P_{ik} + P_{ki} - r_{ik} l_{ik} \quad (9h)$$

$$\dot{r}_{ik} = v_i - v_k - r_{ik} (P_{ik} - P_{ki}) \quad (9i)$$

$$\dot{\rho}_{ik} = \left[P_{ik}^2/v_i - l_{ik} \right]_{\rho_{ik}}^+ \quad (9j)$$

where $G_i(p_i^g) := \frac{\partial}{\partial p_i^g} f_i(p_i^g)$. For any x_i, a_i, b_i with $a_i \leq b_i$, $[x_i]_{a_i}^{b_i} := \min\{b_i, \max\{a_i, x_i\}\}$. Operator $[x_i]_{a_i}^+$ is

$$[x_i]_{a_i}^+ = \begin{cases} x_i, & \text{if } a_i > 0 \text{ or } x_i > 0; \\ 0, & \text{otherwise.} \end{cases}$$

The algorithm (9) is fully distributed where each MG updates its internal states $p_i^g, P_{ik}, l_{ik}, v_i, \hat{p}_i, \mu_i, \epsilon_i, \lambda_{ik}, \gamma_{ik}, \rho_{ik}$ relying only on local information and neighboring information. The neighboring information only appear in variables $P_{ki}, v_k, \rho_{ki}, k \in N_i$. For a microgrid not adopting droop control, \hat{p}_i in (9e) is only a variable in cyber system computed to help controller design. Hence it is feasible to use the hypothesis in practical microgrid operation.

Next, we will investigate the boundedness of $(p_i^g(t), v_i(t))$. Firstly we introduce the assumption

A3: The initial states of the dynamic system (9) are finite, and $(p_i^g(0), v_i(0))$ satisfy constraint (5).

Define the set

$$X := \{(p_i^g, v_i) | 0 \leq p_i^g \leq \bar{p}_i^g, v_i \leq v_i \leq \bar{v}_i\}, \quad (10)$$

then we will prove the boundedness property of $(p_i^g(t), v_i(t))$.

Lemma 2: Suppose assumption A3 holds. Then constraint (5) is satisfied for all $t \geq 0$, i.e., $(p^g(t), v(t)) \in X$ for all $t \geq 0$ where X is defined in (10).

proof (Proof of Lemma 2): Note that (9a) is an inertia link with input

$$u_i^g = [p_i^g - (G_i(p_i^g) - \mu_i + k_i \epsilon_i + z_i + k_i y_i)]_0^{\bar{p}_i^g}$$

According to the feature of inertia link, $p^g(t) \in X$ for all $t \geq 0$ holds as long as $u_i^g(t) \in X$ for all $t \geq 0$. Thus, we know $p^g(t) \in X$ for all $t \geq 0$ always holds. Similarly, $v(t) \in X$ for all $t \geq 0$ always holds. This completes the proof. ■

Lemma 2 implies that inequality constraints are enforced even in the transient for p_i^g and v_i .

B. Optimality of Equilibrium Point

In this subsection, we will prove that the equilibrium points of (9) are primal-dual optimal for ESOCP and its dual, and vice versa. Firstly, the definition of equilibrium points of (9) and the optimal solution of ESOCP are given in Definition 1 and Definition 2 respectively.

Given $x_p := (p^g, P, l, v, \hat{p})$, $x_d := (\mu, \epsilon, \lambda, \gamma, \rho)$, two definitions are introduced.

Definition 1: A point $(x_p^*, x_d^*) := (p^{g*}, P^*, l^*, v^*, \hat{p}^*, \mu^*, \epsilon^*, \lambda^*, \gamma^*, \rho^*)$ is an equilibrium point of (9) if the right-hand side of (9) vanishes at (x_p^*, x_d^*) .

Definition 2: A point (x_p^*, x_d^*) is primal-dual optimal if x_p^* is optimal for ESOCP and x_d^* is optimal for its dual problem.

To prove the optimality of (x_p^*, x_d^*) , we make the following assumption:

A4: Slater's condition for ESOCP holds.

We first illustrate that the saturation of controller does not influence the optimal solution of ESOCP, which is introduced in Lemma 3.

Lemma 3: Suppose A1, A2 and A4 hold. If (x_p^*, x_d^*) is primal-dual optimal, we have

$$p_i^g = [p_i^g - (G_i(p_i^g) - \mu_i^* + k_i \epsilon_i^* + z_i^* + k_i y_i^*)]_0^{p_i^g}$$

$$v_i^* = \left[v_i^* - \left(y_i^* + \sum_{k \in N_i} \gamma_{ik}^* + \epsilon_i^* - \sum_{k \in N_i} \rho_{ik}^* \frac{(P_{ik}^*)^2}{(v_i^*)^2} \right) \right]_{V_i^2}^{V_i^2}$$

The proof of Lemma 3 is given in Appendix B. Based on Lemma 3, we have the following Theorem.

Theorem 3: Suppose A1, A2, A3 and A4 hold. A point (x_p^*, x_d^*) is primal-dual optimal if and only if it is an equilibrium of the dynamic system (9).

The proof of Theorem 3 is given in Appendix B.

C. Convergence Analysis

In this subsection, we will justify the convergence of the algorithm (9) by projection gradient theory combined with invariance principle for switched system.

Define the sets σ_ρ

$$\sigma_\rho := \left\{ (i, k) \in \mathcal{E} \mid \rho_{ik} = 0, P_{ik}^2/v_i - l_{ik} < 0 \right\}$$

Then (9j) is equivalent to

$$\dot{\rho}_{ik} = \begin{cases} \rho_{ik} (P_{ik}^2/v_i - l_{ik}), & \text{if } (i, k) \notin \sigma_\rho; \\ 0, & \text{if } (i, k) \in \sigma_\rho. \end{cases} \quad (11)$$

From (11), it is easy to know $\rho_{ik}(t) \geq 0, \forall t$.

Denote $x := (p_i^g, v_i, P_{ik}, l_{ik}, \hat{p}_i, \mu_i, \epsilon_i, \lambda_{ik}, \gamma_{ik}, \rho_{ik})$ and define $F(x)$ in a fixed σ_ρ .

$$F(x) = \left[\begin{array}{l} G_i(p_i^g) + k_i \epsilon_i - \mu_i + z_i + k_i y_i \\ y_i + \sum_{k \in N_i} \gamma_{ik} + \epsilon_i - \varphi_i^- + \varphi_i^+ - \sum_{k \in N_i} \rho_{ik} \frac{P_{ik}^2}{v_i^2} \\ \mu_i + \lambda_{ik} - \gamma_{ik} r_{ik} + 2 \rho_{ik} \frac{P_{ik}}{v_i} - z_i \\ -\lambda_{ik} r_{ik} - \rho_{ik} - \rho_{ki} \\ -k_i \epsilon_i - k_i y_i \\ p_i^g - p_i^d - \sum_{k \in N_i} P_{ik} \\ -(v_i + k_i p_i^g - v_i^* - k_i \hat{p}_i) \\ -(P_{ik} + P_{ki} - r_{ik} l_{ik}) \\ -(v_i - v_k - r_{ik} (P_{ik} - P_{ki})) \\ -[P_{ik}^2/v_i - l_{ik}]_{\rho_{ik}}^+ \end{array} \right] \quad (12)$$

$F(x)$ is continuously differentiable in a fixed σ_ρ .

We further define the set

$$S := X \times \mathbb{R}^{7m+3n}$$

where X is given in (10). For any x , the projection $x - F(x)$ onto S is

$$H(x) := \text{Proj}_S(x - F(x)) := \arg \min_{y \in S} \|y - (x - F(x))\|_2$$

where $\|\cdot\|_2$ is the Euclidean norm. Then, the algorithm (9) can be rewritten as

$$\dot{x}(t) = H(x(t)) - x(t) \quad (13)$$

A point $x^* \in S$ is an equilibrium of (13) if and only if it is a fixed point of the projection:

$$H(x^*) = x^*$$

Let $E := \{x \in S \mid H(x(t)) - x(t) = 0\}$ be the set of equilibrium points.

Theorem 4: Suppose A1, A2, A3 and A4 hold. Then every trajectory $x(t)$ of (13) starting from a finite initial state asymptotically converges to some equilibrium $x^* \in E$ as $t \rightarrow +\infty$ that is optimal for problem ESOC.

The proof of Theorem 4 is provided in Appendix C.

V. IMPLEMENTATION

Each microgrid may adopt different control strategies: voltage control, power control or droop control. They require different control commands, which are p_i^g, v_i, \hat{p}_i respectively. Since we combine optimization with real time control, values of p_i^g, v_i, \hat{p}_i in the transient process are also sent to the corresponding DGs as the control commands. To distinguish with state variables p_i^g, v_i, \hat{p}_i , control commands sent to DGs are denoted as $p_{gi}^{\text{ref}}, v_i^{\text{ref}}$ and \hat{p}_i^{ref} respectively. For voltage and power control, the algorithm (9) can provide p_{gi}^{ref} and v_i^{ref} that are all feasible even in the transient process. For the droop control microgrids, we can supply \hat{p}_i^{ref} , which ensures the system operate in the optimal status. The control diagrams for three types of microgrid are shown in Fig. 1.

In Fig. 1, the left part is the proposed algorithm, the inputs of which are local information $p_i^g, P_{ik}, l_{ik}, v_i, \hat{p}_i, \mu_i, \epsilon_i, \lambda_{ik}, \gamma_{ik}, \rho_{ik}$ and neighbor information $P_{ki}, v_k, \rho_{ki}, k \in N_i$. The outputs are $p_{gi}^{\text{ref}}, v_i^{\text{ref}}$ and \hat{p}_i^{ref} . The right part is the diagrams of three control strategies: power control, voltage control and droop control. For a power controlled DG, it has two control loops, power loop and current loop, where I_{ref} is the current reference for the current control loop and I_i is the measured current. For a voltage controlled DG, it also has two control loops, power loop and current loop, where v_i is the measured voltage. For a droop controlled DG, it has three control loops, droop control loop, power loop and current loop, where both voltage and current need to be measured.

From Fig. 1, we can see that our method adapts to three commonly used control strategies, which in some sense implies it breaks restriction of various control strategies in microgrids in achieving optimal operation point.

Remark 2: In fact, for microgrid i , neighbor information P_{ki} and v_k can be estimated locally by the following equations

$$P_{ki} = P_{ik} - r_{ik} I_{ik}^2$$

$$v_k = (\sqrt{v_i} - r_{ik} I_{ik})^2$$

where line current I_{ik} from microgrid i to k can be measured locally. Then, only $\rho_{ki}, k \in N_i$ need to be exchanged between neighbors, which implies that the communication burden is minimized.

In the real system, some microgrid may switch off or switch on unexpectedly. The system should also operate optimally in this situation. This requires the controller has the capability of plug-n-play, which will be shown in the simulation.

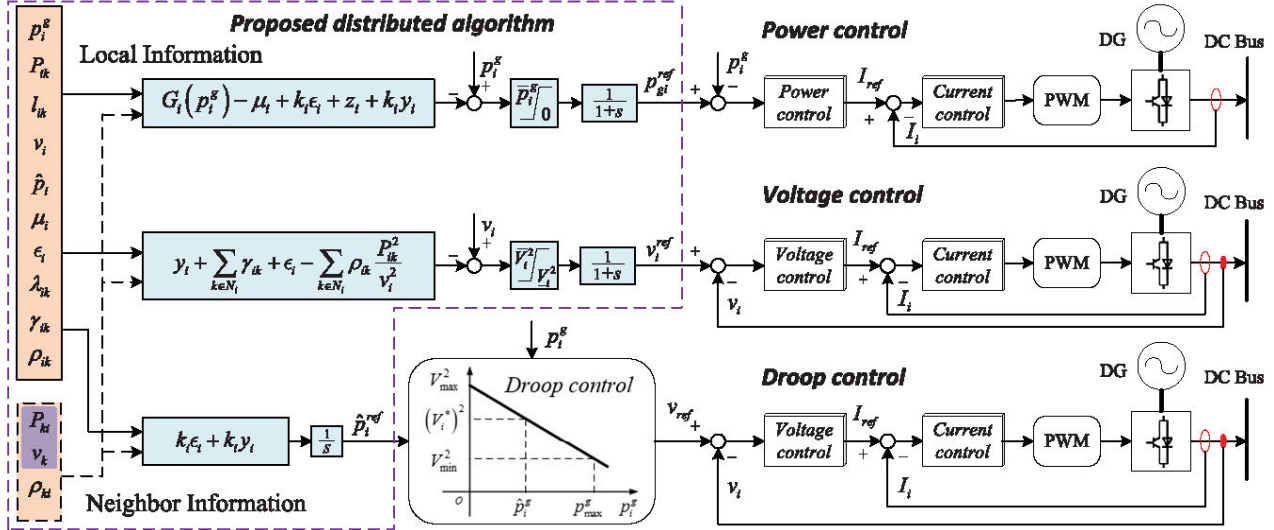


Fig. 1. Control diagram of the proposed method.

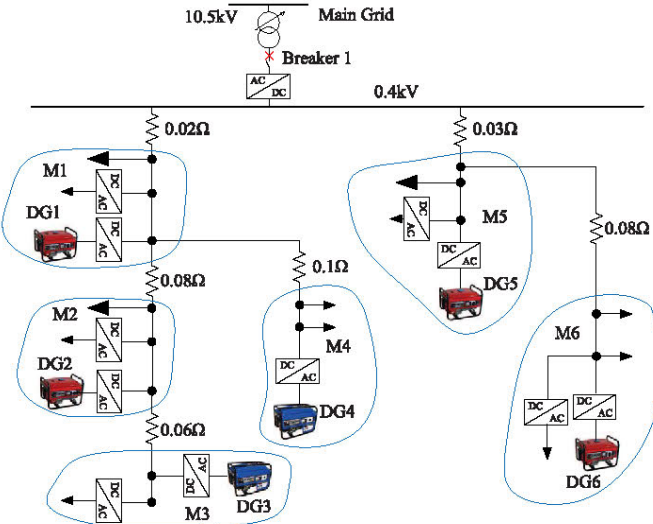


Fig. 2. Six-microgrid system.

VI. CASE STUDIES

A. Test System

To verify the effectiveness of the proposed approach, a multi-microgrid DC system is utilized, the topology of which is based on the low voltage microgrid benchmark in [31]. The system includes two feeders with six dispatchable DGs, which are divided into six microgrids based on corresponding DGs. The Breaker 1 is open, and the system operates in an isolated way. The simulation is performed in PSCAD jointly with MATLAB on a laptop with 8GB memory and 2.39 GHz CPU. More specifically, the DC microgrids are modeled in PSCAD, whereas algorithm (9) is computed in MATLAB. They are combined by a user-defined interface. The control commands obtained in MATLAB are sent to corresponding microgrids in PSCAD through the interface. Conversely, MATLAB can also collect data from PSCAD. In this regard, the PSCAD represents the physical system, while MATLAB represents the

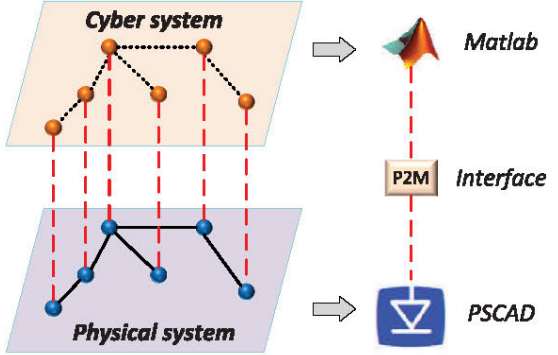


Fig. 3. Simulation design combined with PSCAD and MATLAB.

cyber system. Communication exists in cyber system to obtain the neighborhood information. The joint simulation flowchart is illustrated in Fig. 3. The controller (9) is a continuous form, which needs to be discretized in realization. At each control step, individual local controller only needs to compute a few multiplication and addition operations based on the latest states. In the case studies, it takes only 0.1ms per step, which is fast enough for real-time purpose.

The objective function is set as $f_i(p_i^g) = \frac{a_i}{2}(p_i^g)^2 + b_i p_i^g$, which represents the generation cost of the whole system as the generation cost also takes the quadratic form [27], [32]. If $b_i > 0$, it satisfies A1. Some parameters for these microgrids are provided in Table I. The simulation case is that load demands in each microgrid is (41, 40, 42, 39, 42, 40)kW at first, then they will increase to (51, 50, 52, 49, 52, 50)kW at time 1s. All the three regular control strategies are utilized, i.e, DG1 and DG6 adopt droop control, DG2 and DG5 use power control while DG3 and DG4 adopt voltage control.

B. Accuracy Analysis

In this subsection, we also use CVX tool in MATLAB to solve ESOCP, results of which after load increases are utilized as basic values to validate the accuracy of the proposed

TABLE I
SYSTEM PARAMETERS

	M_1	M_2	M_3	M_4	M_5	M_6
a_i	0.036	0.03	0.035	0.03	0.035	0.042
b_i	1	1	1	1	1	1
p_i^d (kW)	51	50	52	49	52	50
\bar{p}_i^d (kW)	50	60	55	60	55	45
V_i (V)	420	420	420	420	420	420
V_i (V)	380	380	380	380	380	380
k_i	0.12	0.125	0.164	0.131	0.156	0.131

TABLE II
COMPARISON WITH CENTRALIZED OPTIMIZATION

DG _i	Generation (kW)			Power reference (kW)		
	p_g^d	p_g^c	e (%)	\hat{p}^d	\hat{p}^c	e (%)
1	48.1701	48.1823	-0.0253	46.7315	46.8543	-0.2621
2	57.4041	57.4227	-0.0324	56.3536	56.7590	-0.5381
3	49.3516	49.3602	-0.0174	48.2000	48.6611	-0.3311
4	56.9853	56.9861	-0.0014	56.9264	56.9861	-0.1048
5	49.9761	50.0053	-0.0584	48.8660	48.3499	0.4470
6	42.1217	42.1495	-0.0660	39.2465	39.2176	0.0737

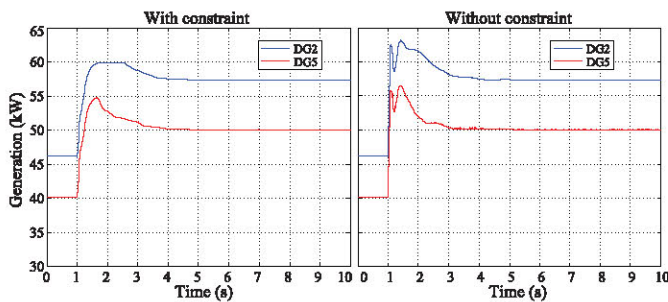


Fig. 4. Generation dynamics with and without constraints.

approach. Results of these two methods are compared in Table II.

In Table II, p_g^d and \hat{p}^d are p_i^s and \hat{p}_i of all DGs obtained by the proposed approach, while p_g^c and \hat{p}^c are values obtained using the CVX tool. e is the errors of p^d and \hat{p}^d with regards to p^c and \hat{p}^c . From results in Table II, it can be seen that the absolute errors between p_g^d and p_g^c in each MGs are smaller than 0.07%. In addition, the absolute errors between \hat{p}^d and \hat{p}^c are smaller than 0.6%. Both validate the accuracy of the proposed approach.

C. Dynamic Process

In this subsection, we analyze the impacts of generation limits on the dynamic property. To do this, we compare dynamic responses of the inverter outputs in M2 and M5 by two scenarios: with and without saturation. The trajectories in two cases are given in Fig. 4. In both cases, the same steady state generations are achieved. However, with the saturated controller, the generations of DG2 and DG5 remain within the limits in both transient and steady state. On the contrary, generations of DG2 and DG5 violate their upper limits in the transient, which is practically infeasible.

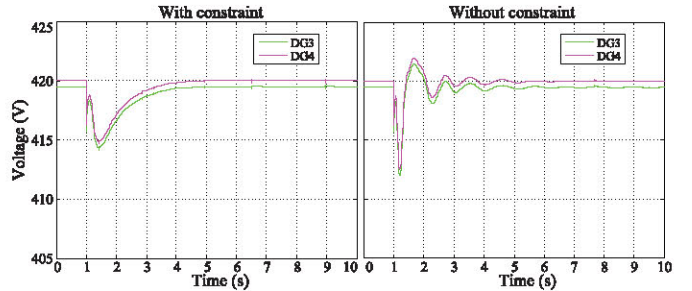


Fig. 5. Voltage dynamics with and without constraints.

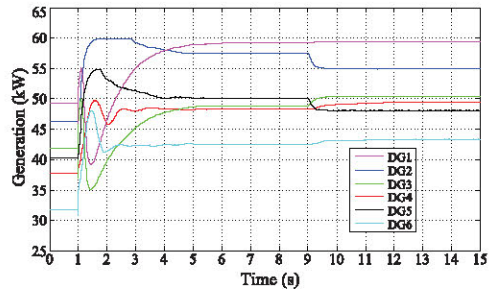


Fig. 6. Generation dynamics of different constraints.

Similarly, we also compare the voltage dynamics of DG3 and DG4 in two scenarios: with and without saturation. The trajectories in two cases are given in Fig. 5. In both cases, the same steady state voltages are achieved. However, with the saturated controller, the voltages of DG3 and DG4 remain within the limits in both transient and steady state. On the contrary, voltages of DG3 and DG4 violate their upper limits in the transient process if saturation is not considered. As we know, the high voltage is both harmful to the power electronic equipments and system operators. In this sense, our method can increase system security.

We reset $\bar{p}_i^d = (60, 55, 60, 65, 48, 50)$ kW at $t = 9$ s, where the power limits of DG2 and DG5 are reduced to 55kW and 48kW respectively. This implies that they can be strictly reached in the steady state. This scenario often happens in microgrids since generation limits of renewable resources such as wind turbines and PVs can change rapidly due to uncertainties. The generations of all DGs with different capacity constraints are given in Fig. 6.

We have checked that generations in Fig. 6 are identical with results obtained by CVX. In Fig. 6, it is shown that generations of DG2 and DG5 reduce rapidly to the capacity limits in the new situation. Other DGs will change their generations to balance the power mismatch in the whole system. This implies our methodology can adapt to disturbances of renewable generations.

In power systems, communication delay always exists, such as transmission, propagation and processing delay, regardless of whether control is centralized or distributed. Fig. 7 shows the dynamics of generation of DG5 and voltage of DG3 under time delays of 5ms, 10ms, 15ms and 35ms. It is shown that the steady state values of both generation and voltage under different time delays are identical, which validates that the

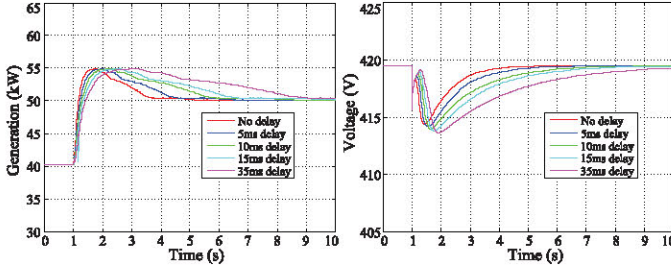


Fig. 7. Generation and voltage dynamics of different time delays.

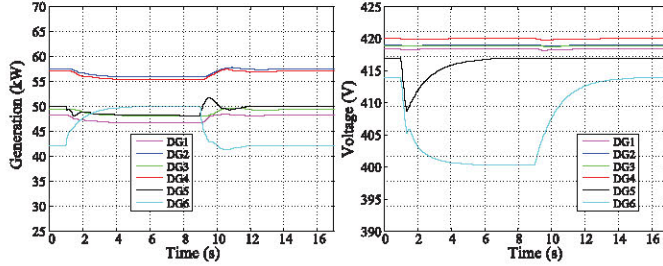


Fig. 8. Generation and voltage dynamics of plug and play.

proposed method can adapt to different time delays and meet real-time requirements. Large delays, however, lead to slower convergence rate and lower voltage nadir.

D. Plug-n-Play Analysis

In this case, M6 is switched off at 1s, then it is switched on at 9s. When M6 is switched off, it has to supply the load demand itself while microgirds 1 to 5 remain connected. Voltage and generation dynamics in the whole process are illustrated in Fig. 8.

It is shown that output of DG6 increases to 50kW to supply the load in M6 after being switched off. At the same time, the voltage of DG6 reduces to 400V. The result is identical with that obtained by CVX. In addition, after M6 is switched on once again, the generations and voltages of all DGs recover to the original values. Moreover, by comparing the voltages in the transient process, it is shown that only the two DGs connected directly with the breaking point are influenced greatly, while other DGs like DG1-DG4 have very moderate transient process. This validates that our controller can realize plug-n-play.

VII. CONCLUSION

This paper addresses the distributed optimal control of stand-alone DC microgrids, where each microgrid may adopt one of the three different control strategies, such as power control, voltage control and droop control. The controller can provide commands for all these strategies, which implies it breaks restriction of various control strategies to achieve optimal operation point. A six-microgrid system based on the microgrid benchmark is utilized to demonstrate the efficacy of our designs. The error of results between proposed method and CVX tool is smaller than 0.6%, which validates the accuracy of the proposed approach. Moreover, the commands for power

controlled and voltage controlled microgrids satisfy generation limits and voltage limits in both transient process and steady state. This increases the security of DC system. In addition, our controller can adapt to the uncertainties of renewable generations. Finally, the proposed approach can realize the plug-n-play.

The tie-line limit is not considered in this work since the convex relaxation may be not exact if it is included. In the normal operation, tie line limit in microgrids is often satisfied by planning stage. However, it is also very important when large disturbance happens. In the future research, we will investigate approaches to addressing this problem.

APPENDIX A PROOFS OF THEOREM 1 AND THEOREM 2

A. Proof of Theorem 1

If A2 holds, problem (7) is also feasible due to the one-to-one map (8). It suffices to prove the uniqueness of the optimal solution of SOCP. Let $x^{1*} = (p^{g1*}, v^{1*}, W^{1*})$ and $x^{2*} = (p^{g2*}, v^{2*}, W^{2*})$ be two optimal solutions of SOCP, then we have

$$\sum_{i \in \mathcal{N}} f_i(p_i^{g1*} - p_i^d) = \sum_{i \in \mathcal{N}} f_i(p_i^{g2*} - p_i^d) \quad (A.1)$$

From the proof of [28, Th. 3], we know

$$\frac{v_i^{1*}}{v_i^{2*}} = \frac{v_k^{1*}}{v_k^{2*}} = \eta, \quad i \sim k$$

$$W_{ik}^{1*} = \sqrt{v_i^{1*} v_k^{1*}} = \eta \sqrt{v_i^{2*} v_k^{2*}} = \eta W_{ik}^{2*}$$

From (4a), we have

$$\begin{aligned} p_i^{g1*} - p_i^d &= \sum_{k: k \sim i} (v_i^{1*} - W_{ik}^{1*}) / r_{ik} \\ &= \sum_{k: k \sim i} (\eta v_i^{2*} - \eta W_{ik}^{2*}) / r_{ik} \\ &= \eta (p_i^{g2*} - p_i^d) \end{aligned}$$

Since $f_i(p_i^g - p_i^d)$ is strictly increasing, we must have $\eta = 1$, otherwise it contradicts (A.1). We have $x^{1*} = x^{2*}$, implying the uniqueness of SOCP solution. According to the one-to-one map (8), solution of SSOCP is also unique. This completes the proof. ■

B. Proof of Theorem 2

⇒ 1) Suppose $x^{1*} = (p^{g1*}, P^{1*}, l^{1*}, v^{1*})$ is the optimal solution of (7), there exists an unique \hat{p}^* satisfying (1). Since two problems have same objective function and constraints except constraint (1), (x^{1*}, \hat{p}^*) is the optimal solution of DSOCP.

⇒ 2) Based on Theorem 1 and assertion 1) of Theorem 2, this assertion is easy to obtain.

⇒ 3) Since $(p^{g2*}, P^{2*}, l^{2*}, v^{2*})$ is the optimal solution of DSOCP, it also satisfies all the constraints of SSOCP. Moreover, DSOCP and SSOCP have identical objective functions, hence $(p^{g2*}, P^{2*}, l^{2*}, v^{2*})$ is the optimal solution of SSOCP. Due to the uniqueness of optimal solution of SSOCP, we have $(p^{g2*}, P^{2*}, l^{2*}, v^{2*}) = (p^{g1*}, P^{1*}, l^{1*}, v^{1*})$. This completes the proof. ■

APPENDIX B
PROOFS OF LEMMA 3 AND THEOREM 3

A. Proof of Lemma 3

With assumption A1, A2 and A4, the strong duality holds. (x_p^*, x_d^*) is the primal-dual optimal if and only if it satisfies the KKT conditions.

The Lagrangian of ESOCOP is given in (B.1).

$$\begin{aligned} L = & \sum_{i \in \mathcal{N}} f_i(p_i^g - p_i^d) + \sum_{i \in \mathcal{N}} \frac{1}{2} z_i^2 + \sum_{i \in \mathcal{N}} \frac{1}{2} y_i^2 \\ & + \sum_{i \in \mathcal{N}} \epsilon_i(v_i + k_i p_i^g - v_i^* - k_i \hat{p}_i) \\ & + \sum_{(i,k) \in \mathcal{E}} \lambda_{ik}(P_{ik} + P_{ki} - r_{ik} l_{ik}) \\ & + \sum_{i \in \mathcal{N}} \gamma_{ik}(v_i - v_k - r_{ik}(P_{ik} - P_{ki})) \\ & + \sum_{(i,k) \in \mathcal{E}} \rho_{ik}(P_{ik}^2/v_i - l_{ik}) \end{aligned} \quad (\text{B.1})$$

Based on (B.1) we can obtain the KKT conditions

$$G_i(p_i^{g*}) - \mu_i^* + k_i \epsilon_i^* + z_i^* + k_i y_i^* \begin{cases} \geq 0, & p_j^{g*} = 0 \\ = 0, & 0 < p_j^{g*} < \bar{p}_j^g \\ \leq 0, & p_j^{g*} = \bar{p}_j^g \end{cases} \quad (\text{B.2a})$$

$$y_i^* + \sum_{k \in \mathcal{N}_i} \gamma_{ik}^* + \epsilon_i^* - \sum_{k \in \mathcal{N}_i} \rho_{ik}^* \frac{(P_{ik}^*)^2}{(v_i^*)^2} \begin{cases} \geq 0, & p_j^{g*} = 0 \\ = 0, & 0 < p_j^{g*} < \bar{p}_j^g \\ \leq 0, & p_j^{g*} = \bar{p}_j^g \end{cases} \quad (\text{B.2b})$$

$$0 = -(\mu_i^* + \lambda_{ik}^* - \gamma_{ik}^* r_{ik} + 2\rho_{ik}^* P_{ik}^*/v_i^* - z_i^*) \quad (\text{B.2c})$$

$$0 = -(-\lambda_{ik}^* r_{ik} - \rho_{ik}^* - \rho_{ki}^*) \quad (\text{B.2d})$$

$$0 = k_i \epsilon_i^* + k_i y_i^* \quad (\text{B.2e})$$

$$0 = -\left(p_i^{*g} - p_i^d - \sum_{k \in \mathcal{N}_i} P_{ik}^*\right) \quad (\text{B.2f})$$

$$0 = v_i^* + k_i p_i^{g*} - v_i^* - k_i \hat{p}_i \quad (\text{B.2g})$$

$$0 = P_{ik}^* + P_{ki}^* - r_{ik} l_{ik}^* \quad (\text{B.2h})$$

$$0 = v_i^* - v_k^* - r_{ik}(P_{ik}^* - P_{ki}^*) \quad (\text{B.2i})$$

$$0 = \left((P_{ik}^*)^2/v_i^* - l_{ik}\right) \rho_{ik}^*, \quad \rho_{ik}^* \geq 0 \quad (\text{B.2j})$$

(x_p^*, x_d^*) is a primal-dual optimal if and only if it satisfies the KKT conditions. It can be checked that (B.2a) and (B.2b) are equivalent to

$$\begin{aligned} p_i^{g*} &= [p_i^{*g} - (G_i(p_i^{*g}) - \mu_i^* + k_i \epsilon_i^* + z_i^* + k_i y_i^*)]_0^{\bar{p}_i^g} \\ v_i^* &= \left[v_i^* - \left(y_i^* + \sum_{k \in \mathcal{N}_i} \gamma_{ik}^* + \epsilon_i^* - \sum_{k \in \mathcal{N}_i} \rho_{ik}^* \frac{(P_{ik}^*)^2}{(v_i^*)^2}\right)\right]_{\underline{V}_i^2}^{\bar{V}_i^2} \end{aligned}$$

This completes the proof. \blacksquare

B. Proof of Theorem 3

\Rightarrow : Suppose (x_p^*, x_d^*) is primal-dual optimal, (x_p^*, x_d^*) satisfies the KKT conditions. It can be obtained directly from (B.2c)-(B.2i) that right sides of dynamics (9c)-(9i) vanish. Right sides of (9a) and (9b) vanish due to Lemma 3.

From (B.2j) and exactness of convex relaxation, we know

$$(P_{ik}^*)^2/v_i^* - l_{ik}^* = 0, \quad \rho_{ik}^* \left((P_{ik}^*)^2/v_i^* - l_{ik}^* \right) = 0$$

Then, the right sides (9j) vanishes. This implies that (x_p^*, x_d^*) is an equilibrium of (9).

\Leftarrow : Suppose (x_p^*, x_d^*) is an equilibrium of (9), then all the right sides of (9) vanish. (9a)-(B.2i) are exactly the KKT conditions (B.2a)-(9i). $\dot{\rho}_{ik} = 0$ implies $\left(\frac{(P_{ik}^*)^2}{v_i^*} - l_{ik}^*\right) \rho_{ik}^*$ and $\rho_{ik}^* \geq 0$, which is identical to (B.2j). Thus, (x_p^*, x_d^*) is primal-dual optimal. This completes the proof. \blacksquare

APPENDIX C
PROOF OF THEOREM 4

Define the following function.

$$\begin{aligned} \tilde{U}(x) &= -F(x)^T \cdot (H(x) - x) \\ &\quad - \frac{1}{2} \|H(x) - x\|_2^2 + \frac{1}{2} \|x - x^*\|_2^2 \end{aligned} \quad (\text{C.1})$$

From [33], we know that $\tilde{U}(x) \geq 0$ and $\tilde{U}(x) = 0$ holds only at any equilibrium point x^* .

For any fixed σ_ρ , \tilde{U} is continuously differentiable as $F(x)$ is continuously differentiable in this situation. Moreover, \tilde{U} is nonincreasing for fixed σ_ρ , as we will prove in Lemma 4. It is worthy to note that the index set σ_ρ may change sometimes, resulting in discontinuity of \tilde{U} [30]. To circumvent such an issue, we slightly modify the definition of \tilde{U} at the discontinuous points as:

- 1) $U(x) := \tilde{U}(x)$, if $\tilde{U}(x)$ is continuous at x ;
- 2) $U(x) := \limsup_{w \rightarrow x} \tilde{U}(w)$, if $\tilde{U}(x)$ is discontinuous at x .

Then $U(x)$ is upper semi-continuous in x , and $U(x) \geq 0$ on S and $U(x) = 0$ holds only at any equilibrium $x^* = H(x^*)$.

Note that U is continuous almost everywhere except the switching points. Hence $U(x)$ is *nonpathological* [34, Definition 3 and 4]. With these definitions and notations above, we can prove Theorem 4.

To prove Theorem 4, we first start with the following lemma.

Lemma 4: Suppose A1, A2 and A3 hold. Then

- 1) $U(x)$ is always decreasing along system (13).
- 2) the trajectory $x(t)$ is bounded.
- 3) every trajectory $x(t)$ starting from a finite initial state ultimately converges to the largest weakly invariant subset Z^* of $Z^+ := \{x \mid \dot{U}(x) = 0\}$.
- 4) every $x^* \in Z^*$ is an equilibrium point of (9).

Proof: In light of [33, Th. 3.2], $U(x)$ is continuously differentiable if $F(x)$ is continuously differentiable. Its gradient is

$$\nabla_x U(x) = F(x) - (\nabla_x F(x) - I)(H(x) - x) + x - x^* \quad (\text{C.2})$$

Then the derivative of $U(x)$ is

$$\dot{U}(x) = \nabla_x^T U(x) \cdot \dot{x} = \nabla_x^T U(x) \cdot (H(x) - x) \quad (\text{C.3})$$

Combining (C.2) and (C.3), we have

$$\begin{aligned}
\dot{U}(x) &= -(H(x) - x)^T \nabla_x F(x) (H(x) - x) \\
&\quad + \langle F(x) + H(x) - x, (H(x) - x) \rangle \\
&\quad + \langle x - x^*, (H(x) - x) \rangle \\
&= \langle F(x) + H(x) - x, H(x) - x^* + x^* - x \rangle \\
&\quad + \langle x - x^*, H(x) - x \rangle \\
&\quad - (H(x) - x)^T \nabla_x F(x) (H(x) - x) \\
&= \langle F(x) + H(x) - x, H(x) - x^* \rangle \tag{C.4a} \\
&\quad + \langle x - x^*, -F(x) \rangle \tag{C.4b} \\
&\quad - (H(x) - x)^T \nabla_x F(x) (H(x) - x) \tag{C.4c}
\end{aligned}$$

$$+ \langle x - x^*, -F(x) \rangle \quad (C.4b)$$

$$- (H(x) - x)^T \nabla_x F(x) (H(x) - x) \quad (\text{C.4c})$$

Next, we will prove that (C.4a), (C.4b) and (C.4c) are all nonpositive. For ξ and χ , the projection has the following property [33]

$$\langle \xi - \text{Proj}(\xi)s, \chi - \text{Proj}(\xi)s \rangle \leq 0 \quad \forall \chi \in S$$

Set $\xi = x - F(x)$, $\chi = x^*$, then we have

$$\langle F(x) + H(x) - x, H(x) - x^* \rangle \leq 0. \quad (\text{C.5})$$

This implies that (C.4a) is nonpositive.

Write $x_1 := (p_i^g, v_i, P_{ik}, l_{ik}, \hat{p}_i)$ and $x_2 := (\mu_i, \epsilon_i, \lambda_{ik}, \gamma_{ik}, \rho_{ik})$, then L is convex in x_1 and concave in x_2 . It can be verified that

$$\begin{aligned}
\langle x - x^*, -F(x) \rangle &= -(x_1 - x_1^*)^T \nabla_{x_1}^T L + (x_2 - x_2^*)^T \nabla_{x_2}^T L \\
&\leq L(x_1^*, x_2) - L(x_1, x_2) + L(x_1, x_2) - L(x_1, x_2^*) \\
&= \underbrace{L(x_1^*, x_2) - L(x_1^*, x_2^*)}_{\leq 0} + \underbrace{L(x_1^*, x_2^*) - L(x_1, x_2^*)}_{\leq 0} \\
&\leq 0
\end{aligned} \tag{C.6}$$

This implies that (C.4b) is nonpositive.

For (C.4c), we have

$$\begin{aligned}
 - (H(x) - x)^T \nabla_x F(x) (H(x) - x) &= -\dot{x}^T \nabla_x F(x) \dot{x} \\
 &= -\dot{x}^T Q \dot{x} \\
 &\leq 0
 \end{aligned} \tag{C.7}$$

where Q is given in (C.8), as shown at the bottom of this page with

$$\begin{aligned}
M_n &= \text{diag} \left(\sum_{k \in N_i} \frac{2\rho_{ik} P_{ik}^2}{v_i^3} \right) \\
T_{n \times 2m}(s, t) &= \begin{cases} 1, & \text{if } (s, t+1) \in \mathcal{E} \text{ or } (s, t-m+1) \in \mathcal{E} \\ 0, & \text{otherwise} \end{cases} \\
D_{n \times 2m}(s, t) &= \begin{cases} -\frac{2\rho_{s,t+1} P_{s,t+1}}{v_s^2}, & \text{if } (s, t+1) \in \mathcal{E} \\ & \text{or } (s, t-m+1) \in \mathcal{E} \\ 0, & \text{otherwise} \end{cases} \\
R_{n \times 2m}(s, t) &= \begin{cases} -\frac{P_{s,t+1}^2}{v_s^2}, & \text{if } (s, t+1) \in \mathcal{E} \\ & \text{or } (s, t-m+1) \in \mathcal{E} \\ 0, & \text{otherwise} \end{cases} \\
\tilde{I}_{m \times 2m}^1(s, t) &= \begin{cases} 1, & \text{if } (s, t+1) \in \mathcal{E} \text{ or } (s, t-m+1) \in \mathcal{E} \\ 0, & \text{otherwise} \end{cases} \\
\tilde{I}_{m \times 2m}^2(s, t) &= \begin{cases} 1, & \text{if } (s, t+1) \in \mathcal{E} \text{ and } s \leq t \\ -1, & \text{if } (s, t-m+1) \in \mathcal{E} \text{ and } s > t-m \\ 0, & \text{otherwise} \end{cases}
\end{aligned}$$

Q is a semi-definite positive matrix. I is a identity matrix, the subscript implies its dimension. $[c_i]_d$ denotes the diagonal matrix composed of c_i with proper dimensions. Moreover, Q can be divided into two matrices, one of which is skew-symmetric and the other is positive symmetric.

Note that the index set σ_ρ may change during the decreasing of U . We have the following observations:

- The set σ_ρ is reduced, which only happens when $P_{ik}^2/v_i - l_{ik}$ goes through zero, from negative to positive. Hence an extra term will be added to U . As this term is initially zero, there is no discontinuity of U in this case.
- The set σ_ρ is enlarged when ρ_{ik} goes to zero from positive while $P_{ik}^2/v_i - l_{ik} \leq 0$. Here U will lose a positive term $\left(\frac{P_{ik}^2}{v_i} - l_{ik}\right)^2/2$, causing discontinuity.

Hence, U keeps decreasing even when σ_ρ changes, which implies 1) of Lemma 4. In addition, note that [33, Th. 3.1] proves that $-F(x)^T(H(x) - x) - \frac{1}{2}\|H(x) - x\|_2^2 \geq 0$.

Therefore, we have

$$\frac{1}{2} \|x - x^*\|_2^2 \leq U(t) \leq U(0)$$

which implies that $x(t)$ is bounded. Then, 2) of Lemma 4 holds.

Given an initial point $x(0)$ there is a compact set $\Omega_0 := \Omega(x(0)) \subset S$ such that $x(t) \in \Omega_0$ for $t \geq 0$ and $\dot{U}(x) \leq 0$ in Ω_0 .

In addition, U is radially unbounded and positively definite except at equilibrium. As U and \dot{U} are nonpathological, we conclude that any trajectory $x(t)$ starting from Ω_0 converges to the largest weakly invariant subset Z^* contained in $Z^+ = \{x \in \Omega_0 \mid \dot{U}(x) = 0\}$ [34, Proposition 3], proving the third assertion.

Now, we will prove the last assertion of Lemma 4. To satisfy $\dot{U}(x) = 0$, both terms in (C.6) have to be zero, implying that

$$L(x_1^*, x_2) \equiv L(x_1^*, x_2^*)$$

must hold in Z^+ . Differentiating with respect to t gives

$$\left(\frac{\partial}{\partial x_2} L(x_1^*, x_2(t)) \right)^T \cdot \dot{x}_2(t) = 0 = \dot{x}_2(t)^T \dot{x}_2(t) \quad (\text{C.9})$$

The second equality holds due to (9f)-(9j). Then, we can conclude $\dot{x}_2(t) = 0$ due to the boundedness of $x(t)$, which implies that $\mu_i, \epsilon_i, \lambda_{ik}, \gamma_{ik}, \rho_{ik}$ are constants and $y_i = z_i = 0$ in Z^+ . We can obtain $\dot{l}_{ik} = \dot{p}_i = 0$ from (9d), (9e) as well as the boundedness of $x(t)$.

Combining (C.7) and (C.8), we have

$$\begin{aligned} \dot{U}(x) &\leq -\dot{x}^T Q \dot{x} \\ &= -\sum_{i \in \mathcal{N}} (\dot{p}_i^g)^T \cdot \nabla_{p_i^g} f \cdot \dot{p}_i^g - \sum_{i \in \mathcal{N}} \left(\dot{p}_i^g - \sum_{k \in \mathcal{N}_i} \dot{P}_{ik} \right)^2 \\ &\quad - \sum_{i \in \mathcal{N}} \frac{2\rho_{ik}}{v_i} \left(\dot{P}_{ik} - \sum_{k \in \mathcal{N}_i} \frac{|P_{ik}|}{v_i} \dot{v}_i \right)^2 \\ &\quad - \sum_{i \in \mathcal{N}} \left(\dot{v}_i + k_i \dot{p}_i^g - k_i \dot{p}_i \right)^2 \end{aligned} \quad (\text{C.10})$$

We can directly get $\dot{p}_i^g = 0$ due to the A1. From $\dot{v}_i + k_i \dot{p}_i^g - k_i \dot{p}_i = 0$ and $\dot{p}_i^g = \dot{p}_i = 0$, we have $\dot{v}_i = 0$. If $\rho_{ik} = 0$, then \dot{P}_{ik} is a constant, implying $\dot{P}_{ik} = 0$. If $\rho_{ik} > 0$, then $\frac{\dot{P}_{ik}^2}{v_i} = l_{ik}$, implying P_{ik} a constant. Thus, $\dot{P}_{ik} = 0$ always holds. Consequently, we have that $\dot{x}(t) = 0$ in Z^* , which is the last assertion of Lemma 4. ■

Proof of Theorem 4: Fix any initial state $x(0)$ and consider the trajectory $(x(t), t \geq 0)$ of (13). As mentioned in the proof of Lemma 4, $x(t)$ stays entirely in a compact set Ω_0 . Hence there exists an infinite sequence of time instants t_k such that $x(t_k) \rightarrow \hat{x}^*$ as $t_k \rightarrow \infty$, for some $\hat{x}^* \in Z^*$. The 4) in Lemma 4 guarantees that \hat{x}^* is an equilibrium point of the (13), and hence $\hat{x}^* = H(\hat{x}^*)$. Thus, using this specific equilibrium point \hat{x}^* in the definition of U , we have

$$\begin{aligned} U^* &= \lim_{t \rightarrow \infty} U(x(t)) = \lim_{t_k \rightarrow \infty} U(x(t_k)) \\ &= \lim_{x(t_k) \rightarrow \hat{x}^*} U(x(t_k)) = U(\hat{x}^*) = 0 \end{aligned}$$

Here, the first equality uses the fact that $U(t)$ is nonincreasing in t ; the second equality uses the fact that t_k is the infinite sequence of t ; the third equality uses the fact that $x(t)$ is absolutely continuous in t ; the fourth equality is due to the upper semi-continuity of $U(x)$, and the last equality holds as \hat{x}^* is an equilibrium point of $U(x)$.

The quadratic term $(x - \hat{x}^*)^T (x - \hat{x}^*)$ in $U(x)$ then implies that $x(t) \rightarrow \hat{x}^*$ as $t \rightarrow \infty$, which completes the proof. ■

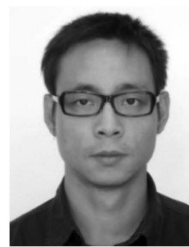
REFERENCES

- [1] J. J. Justo, F. Mwasilu, J. Lee, and J.-W. Jung, "AC-microgrids versus DC-microgrids with distributed energy resources: A review," *Renew. Sustain. Energy Rev.*, vol. 24, pp. 387–405, Aug. 2013.
- [2] E. Planas, J. Andreu, J. I. Gárate, I. M. de Alegria, and E. Ibarra, "AC and DC technology in microgrids: A review," *Renew. Sustain. Energy Rev.*, vol. 43, pp. 726–749, Mar. 2015.
- [3] T. Dragičević, X. Lu, J. C. Vasquez, and J. M. Guerrero, "DC microgrids—Part I: A review of control strategies and stabilization techniques," *IEEE Trans. Power Electron.*, vol. 31, no. 7, pp. 4876–4891, Jul. 2016.
- [4] T. Dragičević, X. Lu, J. C. Vasquez, and J. M. Guerrero, "DC microgrids—Part II: A review of power architectures, applications, and standardization issues," *IEEE Trans. Power Electron.*, vol. 31, no. 5, pp. 3528–3549, May 2016.
- [5] A. T. Elsayed, A. A. Mohamed, and O. A. Mohammed, "DC microgrids and distribution systems: An overview," *Elect. Power Syst. Res.*, vol. 119, pp. 407–417, Feb. 2015.
- [6] J. M. Guerrero, J. C. Vasquez, J. Matas, L. G. de Vicuna, and M. Castilla, "Hierarchical control of droop-controlled AC and DC microgrids—A general approach toward standardization," *IEEE Trans. Ind. Electron.*, vol. 58, no. 1, pp. 158–172, Jan. 2011.
- [7] Q. Shafiee, T. Dragičević, J. C. Vasquez, and J. M. Guerrero, "Hierarchical control for multiple DC-microgrids clusters," *IEEE Trans. Energy Convers.*, vol. 29, no. 4, pp. 922–933, Dec. 2014.
- [8] M. Yazdanian and A. Mehrizi-Sani, "Distributed control techniques in microgrids," *IEEE Trans. Smart Grid*, vol. 5, no. 6, pp. 2901–2909, Nov. 2014.
- [9] A. Maknooninejad, Z. Qu, F. L. Lewis, and A. Davoudi, "Optimal nonlinear, and distributed designs of droop controls for DC microgrids," *IEEE Trans. Smart Grid*, vol. 5, no. 5, pp. 2508–2516, Sep. 2014.
- [10] A. Khorsandi, M. Ashourloo, and H. Mokhtari, "A decentralized control method for a low-voltage DC microgrid," *IEEE Trans. Energy Convers.*, vol. 29, no. 4, pp. 793–801, Dec. 2014.
- [11] Y. Gu, X. Xiang, W. Li, and X. He, "Mode-adaptive decentralized control for renewable DC microgrid with enhanced reliability and flexibility," *IEEE Trans. Power Electron.*, vol. 29, no. 9, pp. 5072–5080, Sep. 2014.
- [12] D. Chen and L. Xu, "Autonomous DC voltage control of a DC microgrid with multiple slack terminals," *IEEE Trans. Power Syst.*, vol. 27, no. 4, pp. 1897–1905, Nov. 2012.
- [13] M. D. Cook, G. G. Parker, R. D. Robinett, and W. W. Weaver, "Decentralized mode-adaptive guidance and control for DC microgrid," *IEEE Trans. Power Del.*, vol. 32, no. 1, pp. 263–271, Feb. 2017.
- [14] X. Lu, K. Sun, J. M. Guerrero, J. C. Vasquez, and L. Huang, "State-of-charge balance using adaptive droop control for distributed energy storage systems in DC microgrid applications," *IEEE Trans. Ind. Electron.*, vol. 61, no. 6, pp. 2804–2815, Jun. 2014.
- [15] R. Olfati-Saber, J. A. Fax, and R. M. Murray, "Consensus and cooperation in networked multi-agent systems," *Proc. IEEE*, vol. 95, no. 1, pp. 215–233, Jan. 2007.
- [16] Q. Shafiee, T. Dragicevic, F. Andrade, J. C. Vasquez, and J. M. Guerrero, "Distributed consensus-based control of multiple DC-microgrids clusters," in *Proc. 40th Annu. Conf. IEEE Ind. Electron. Soc. (IECON)*, Dallas, TX, USA, Oct. 2014, pp. 2056–2062.
- [17] V. Nasirian, S. Moayedi, A. Davoudi, and F. L. Lewis, "Distributed cooperative control of DC microgrids," *IEEE Trans. Power Electron.*, vol. 30, no. 4, pp. 2288–2303, Apr. 2015.
- [18] Z. Lv, Z. Wu, X. Dou, and M. Hu, "Discrete consensus-based distributed secondary control scheme with considering time-delays for DC microgrid," in *Proc. 41st Annu. Conf. IEEE Ind. Electron. Soc. (IECON)*, Yokohama, Japan, Nov. 2015, pp. 002898–002903.
- [19] L. Che and M. Shahidehpour, "DC microgrids: Economic operation and enhancement of resilience by hierarchical control," *IEEE Trans. Smart Grid*, vol. 5, no. 5, pp. 2517–2526, Sep. 2014.

- [20] J. Xiao, P. Wang, and L. Setyawan, "Hierarchical control of hybrid energy storage system in DC microgrids," *IEEE Trans. Ind. Electron.*, vol. 62, no. 8, pp. 4915–4924, Aug. 2015.
- [21] S. Moayedi and A. Davoudi, "Distributed tertiary control of DC microgrid clusters," *IEEE Trans. Power Electron.*, vol. 31, no. 2, pp. 1717–1733, Feb. 2016.
- [22] C. Zhao, U. Topcu, N. Li, and S. H. Low, "Design and stability of load-side primary frequency control in power systems," *IEEE Trans. Autom. Control*, vol. 59, no. 5, pp. 1177–1189, May 2014.
- [23] N. Li, C. Zhao, and L. Chen, "Connecting automatic generation control and economic dispatch from an optimization view," *IEEE Trans. Control Netw. Syst.*, vol. 3, no. 3, pp. 254–264, Sep. 2016.
- [24] F. Dörfler, J. W. Simpson-Porco, and F. Bullo, "Breaking the hierarchy: Distributed control and economic optimality in microgrids," *IEEE Trans. Control Netw. Syst.*, vol. 3, no. 3, pp. 241–253, Sep. 2016.
- [25] S. Moayedi and A. Davoudi, "Unifying distributed dynamic optimization and control of islanded dc microgrids," *IEEE Trans. Power Electron.*, vol. 32, no. 3, pp. 2329–2346, Mar. 2017.
- [26] A. A. Hamad, M. A. Azzouz, and E. F. El-Saadany, "Multiagent supervisory control for power management in DC microgrids," *IEEE Trans. Smart Grid*, vol. 7, no. 2, pp. 1057–1068, Mar. 2016.
- [27] Z. Wang, W. Wu, and B. Zhang, "A distributed control method with minimum generation cost for DC microgrids," *IEEE Trans. Energy Convers.*, vol. 31, no. 4, pp. 1462–1470, Dec. 2016.
- [28] L. Gan and S. H. Low, "Optimal power flow in direct current networks," *IEEE Trans. Power Syst.*, vol. 29, no. 6, pp. 2892–2904, Nov. 2014.
- [29] J. Li, F. Liu, Z. Wang, S. Low, and S. Mei, "Optimal power flow in stand-alone DC microgrids," *arXiv preprint arXiv:1708.05140*, 2017.
- [30] D. Feijer and F. Paganini, "Stability of primal-dual gradient dynamics and applications to network optimization," *Automatica*, vol. 46, no. 12, pp. 1974–1981, Dec. 2010.
- [31] S. Papathanassiou, N. Hatzigyriou, and K. Strunz, "A benchmark low voltage microgrid network," in *Proc. CIGRE Symp. Power Syst. Dispersed Gener.*, 2005, pp. 1–8.
- [32] Y. Xu and Z. Li, "Distributed optimal resource management based on the consensus algorithm in a microgrid," *IEEE Trans. Ind. Electron.*, vol. 62, no. 4, pp. 2584–2592, Apr. 2015.
- [33] M. Fukushima, "Equivalent differentiable optimization problems and descent methods for asymmetric variational inequality problems," *Math. Program.*, vol. 53, nos. 1–3, pp. 99–110, Jan. 1992.
- [34] A. Bacciotti and F. Ceragioli, "Nonpathological Lyapunov functions and discontinuous carathéodory systems," *Automatica*, vol. 42, no. 3, pp. 453–458, 2006.



Zhaojian Wang (S'15) received the B.S. degree from the Qishu Honors College, Tianjin University, Tianjin, China, in 2013. From 2016 to 2017, he was a joint Ph.D. student with the California Institute of Technology, CA, USA. He is currently pursuing the Ph.D. degree in electrical engineering with Tsinghua University, Beijing, China. His research interests include power system distributed optimal control and microgrid planning.



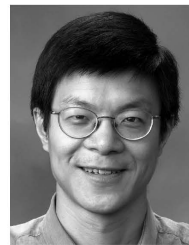
Feng Liu (M'12) received the B.Sc. and Ph.D. degrees in electrical engineering from Tsinghua University, Beijing, China, in 1999 and 2004, respectively.

He is currently an Associate Professor with Tsinghua University. From 2015 to 2016, he was a Visiting Associate with the California Institute of Technology, CA, USA. He has authored/co-authored over 100 peer-reviewed technical papers and two books, and holds over 20 issued/pending patents. His research interests include power system stability analysis, optimal control and robust dispatch, game theory and learning theory and their applications to smart grids. He is a Guest Editor of the IEEE TRANSACTIONS ON ENERGY CONVERSION.



Ying Chen (M'07) received the B.E. and Ph.D. degrees in electrical engineering from Tsinghua University, Beijing, China, in 2001 and 2006, respectively.

He is currently an Associate Professor with the Department of Electrical Engineering and Applied Electronic Technology, Tsinghua University. His research interests include parallel and distributed computing, electromagnetic transient simulation, cyber-physical system modeling, and cyber security of smart grid.



Steven H. Low (F'08) received the B.S. degree from Cornell University, Ithaca, NY, USA, in 1987, and the Ph.D. degree from the University of California, Berkeley, CA, USA, in 1992, both in electrical engineering.

He was with AT&T Bell Laboratories, Murray Hill, NJ, USA, and the University of Melbourne, Australia. He is a Professor of the Department of Computing and Mathematical Sciences and the Department of Electrical Engineering, California Institute of Technology, Pasadena, CA, USA. He has authored the book entitled *Analytical Methods for Network Congestion Control* (Morgan & Claypool, 2017). He is a Senior Editor of the IEEE TRANSACTIONS ON CONTROL OF NETWORK SYSTEMS, and on the editorial board of NOW Foundations and Trends in Networking, and in Power Systems, as well as that of the *Journal of Sustainable Energy, Grids and Networks*.



Shengwei Mei (SM'05–F'15) received the B.S. degree in mathematics from Xinjiang University, Urumqi, China, in 1984, the M.S. degree in operations research from Tsinghua University, Beijing, China, in 1989, and the Ph.D. degree in automatic control from the Chinese Academy of Sciences, Beijing, in 1996.

He is currently a Professor with the Department of Electrical Engineering, Tsinghua University. His research interests include power system analysis and control, robust control, and complex systems.